Computational Modeling of Single-Cell Migration:

Schlueter, Daniela K.; Ramis-Conde, Ignacio; Chaplain, Mark A. J.

Published in:
Biophysical Journal

DOI:
10.1016/j.bpj.2012.07.048

Publication date:
2012

Document Version
Publisher's PDF, also known as Version of record

Computational Modeling of Single-Cell Migration: The Leading Role of Extracellular Matrix Fibers

Daniela K. Schlüter,[†*] Ignacio Ramis-Conde,[‡] and Mark A. J. Chaplain[†]
[†]Division of Mathematics, University of Dundee, Dundee, Scotland; and [‡]Department of Mathematics, Faculty of Education, Universidad de Castilla la Mancha, Cuenca, Spain

ABSTRACT Cell migration is vitally important in a wide variety of biological contexts ranging from embryonic development and wound healing to malignant diseases such as cancer. It is a very complex process that is controlled by intracellular signaling pathways as well as the cell's microenvironment. Due to its importance and complexity, it has been studied for many years in the biomedical sciences, and in the last 30 years it also received an increasing amount of interest from theoretical scientists and mathematical modelers. Here we propose a force-based, individual-based modeling framework that links single-cell migration with matrix fibers and cell-matrix interactions through contact guidance and matrix remodelling. With this approach, we can highlight the effect of the cell's environment on its migration. We investigate the influence of matrix stiffness, matrix architecture, and cell speed on migration using quantitative measures that allow us to compare the results to experiments.

INTRODUCTION

The migration of individual cells occurs in a wide variety of biological contexts ranging from development and wound healing to malignant diseases such as cancer (1–4). To migrate, a cell first needs to acquire front-rear polarity, which in itself is a very complex process (5,6). The direction in which a cell polarizes can be determined by extracellular cues such as growth factors, chemical gradients, and extracellular matrix (ECM) components, through spatially limited activation of signaling complexes (7). The polarity is stabilized and sustained during migration by multiple feedback mechanisms, including integrins, which are cell-matrix adhesion molecules that maintain the spatial molecular asymmetry (1,7). Complexes at the front of the cell interact with the actin cytoskeleton, leading to polymerization and extended membrane protrusions (7,8). These lamellipodia or filopodia then bind to the ECM through integrins that cluster to form small, dot-like focal complexes (9). Over a timescale of minutes (10), the focal complexes can then develop into stable focal contacts that give the cell traction (9,11). Cell contraction then leads to the generation of traction forces and hence the forward movement of the cell body, releasing any cell-matrix bonds at the rear of the cell (1,10,12,13). Cell migration in a three-dimensional (3D) matrix additionally requires focalized proteolysis (12).

A key component of all cell migration is the interaction with the individual fibers of the matrix, and experimental studies have investigated the importance of remodeling of individual fibers, cell adhesion, and force generation on 2D surfaces (14–19). Images of actual individual cells migrating through 2D matrices are shown in Fig. 1. These images clearly show individual cells interacting with and reorienting single fibers (see Fig. 1), and such processes are the focus of the modeling efforts in this work.

Theoretical modeling approaches in this area have already provided insights into this complex process. Such approaches include models at the level of intracellular actin dynamics at the leading edge of motile cells (20,21), and detailed models of single-cell mechanics during migration (13,22), which were able to predict the speed of migrating cells and the biphasic dependence on multiple factors, such as receptor and ligand densities. Hybrid discrete-continuum (23,24) and continuum (25–27) models of cell migration in 2D and 3D matrices have elucidated the impact of the ECM on cell migration. However, there is still a vast area to explore concerning specific cell-matrix interactions and the influence of individual matrix fibers on migration. In this work, we propose a fully individual-based modeling framework of cell migration. Whenever possible, we use example parameter values from experimental literature. In cases for which no data are available, we use estimates and nondimensional values to arrive at biologically insightful results. However, given data on specific cell types, matrices, and cell-matrix interaction forces, the model can easily be adapted and can give quantitative results for these particular cases.

MODEL DESCRIPTION AND DATA ANALYSIS

We developed an individual-based model of cell migration that is driven by forces acting on the cell. In addition, individual matrix fibers are reoriented due to cell traction forces. We focus on the migration of single cells on 2D substrates. Our force-based modeling approach is similar to the one

Submitted October 19, 2011, and accepted for publication July 24, 2012.

*Correspondence: dkschlueter@maths.dundee.ac.uk

Editor: Leah Edelstein-Keshet.

0006-3495/12/09/1141/11 $2.00

http://dx.doi.org/10.1016/j.bpj.2012.07.048

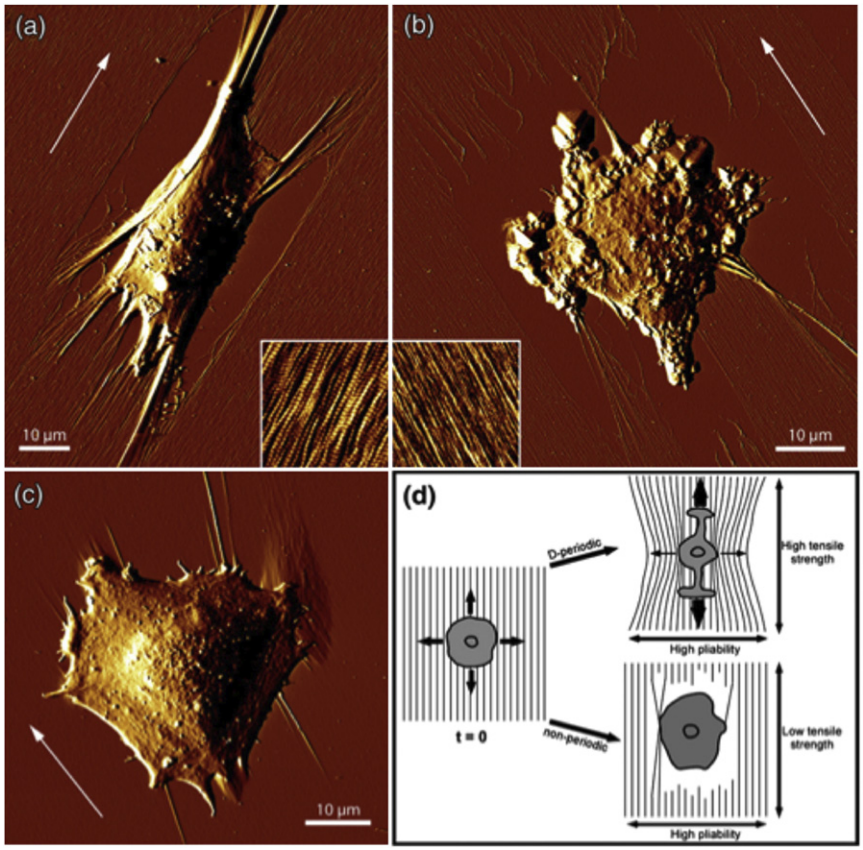

FIGURE 1 Experimental images of individual cells interacting with collagen matrices with different fiber alignments. (*a*) D-periodic fibers (i.e., anisotropic). (*b*) Nonperiodic fibers (i.e., isotropic). (*c*) Glutaraldehyde-fixed D-periodic fibers. Reproduced with copyright permission from Friedrichs et al. (14).

previously used to study epithelial cell populations (28), cancer cell invasion (29), the process of intravasation (30), and cell migration in 3D matrices without the explicit inclusion of matrix elements (22).

Modeling the cell and the ECM

The shape of an individual cell is relatively flat and hemispherical, and we assume a radius of the base of 15 μm and a height of 2.6 μm, as previously measured for Madin-Darby canine kidney (MDCK) cells by Schneider et al. (31). We explicitly model individual matrix fibers, which could represent fibronectin, collagen, laminin, or other fibrous matrix components. These fibers are represented by thin cylinders with lengths that are normally distributed with a mean of 75 μm and standard deviation (SD) of 5 μm, and width of 200 nm (e.g., as measured for collagen by Friedl et al. (32)). We consider a spatial domain of size 1000 $\times$ 1000 μm in which we place 15,000 fibers, one of the endpoints of which is randomly positioned following a uniform distribution in space. For isotropic matrices, the direction of each fiber is given by a normalized vector with uniformly distributed x and y components (see Fig. 2 *a*). Ordered matrices are also generated in which the matrix fibers are either biased in the sense that they form an angle between 90° and 180° with the x axis or are fully aligned so that the direction of the fibers forms a 135° angle with the x axis (see Fig. 2, *b* and *c*).

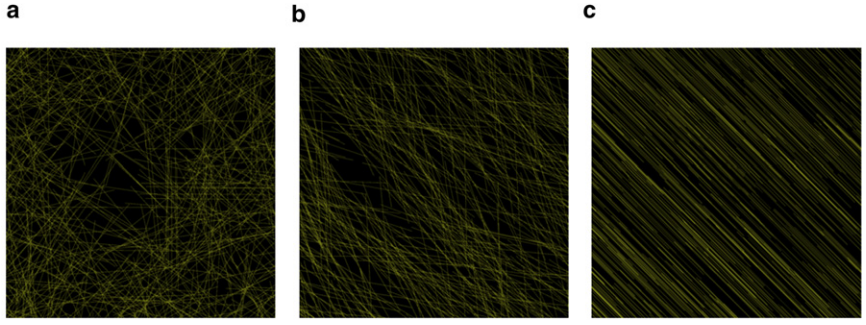

FIGURE 2 Computer-generated initial extracellular matrices with (*a*) randomly distributed fibers, (*b*) biased fibers, and (*c*) aligned fibers. The figure shows a representative 150×150 μm square subdomain taken from the entire domain of size 1000×1000 μm.

Modeling the cell movement

Cell movement is governed by the total forces acting on an individual cell. By calculating all of the forces acting on a cell and then applying Newton's law of motion (ignoring inertia terms (28,29)), we obtain an equation for the cell velocity. Integrating this equation, we can then calculate the displacement of an individual cell over time. The system we are modeling consists of individual cells interacting with individual matrix fibers, and so the forces on an individual cell consist of a drag force that is balanced by the overall force generated by an individual cell through contact with the matrix fibers and a term accounting for underlying noise. Therefore, the governing equation of motion has the general form:

$$\mathbf{F}_{drag} = \sum_{f} \mathbf{F}_{fj} + \mathbf{f}_j(t). \quad (1)$$

The drag force $\mathbf{F}_{drag}$ is calculated using a variation of Stokes' law for nonspherical objects as developed previously (33,34). This includes a shape factor that is based on the assumption that the cell has a symmetric hemispherical shape. $\mathbf{F}_{fj}$ is the force generated by an individual cell through contact with an individual matrix fiber, with the sum taken over the fibers that are in contact with the cell. Thus, $\sum_f \mathbf{F}_{fj}$ is calculated from the directions and number of matrix fibers with which a cell is in contact. $\mathbf{f}_j(t)$ is the term that accounts for noise that is uncorrelated and has zero mean. All of these terms are explained and derived in detail in the Supporting Material.

Modeling the matrix rearrangement due to cell traction forces

Upon cell contraction during migration, traction forces are transmitted to the substrate through the adhesion complexes, and the pulling on the fibers realigns the matrix (1,12) (see Fig. 1). These traction forces of a cell point toward its center (35,36) and thus the fiber is pulled inward. We model the fiber as a lever that is rotated about its moment of force. With this assumption, the end of the fiber that is farthest away from the cell acts as the fulcrum. We assume that the realignment of the fiber is proportional to the integrin expression of the cell and is inversely proportional to the matrix stiffness, which is a nondimensional value between zero and one. The realignment becomes smaller the closer the fiber is to the cell's midpoint, as the traction forces become smaller from the cell's periphery inward (35,36). Under these assumptions, the angle of rotation ϕ of a fiber is given by

$$\phi = \Theta - \arcsin\left(\frac{(1 - 0.1 \times I \cdot (1 - S)) \cdot D}{d}\right) \quad (2)$$

where Θ is the current angle between the straight line connecting the fulcrum and the cell's midpoint and the fiber, I is the percentage of integrins expressed by the cell, S is the matrix stiffness, D is the shortest distance between the fiber and the cell, and d is the distance of the fulcrum from the cell's midpoint. The other parameter used, the factor 0.1, was estimated to give an appropriate reduction of the reorientation per time step. However, a 10% or 20% change of this parameter does not affect the results (see Fig. S7). The change in ϕ and Θ over five simulation time steps for different matrix stiffnesses can be seen in Fig. S3, *a* and *b*.

The matrix stiffness S can either be a constant value throughout the domain or, more realistically, we can calculate it for each fiber depending on the number of fibers with which it has cross-links. For <15 cross-links, we assume a matrix stiffness of the number of cross-links $\times$ 0.06. For >15 cross-links, the fiber is assigned a stiffness of 0.95. This maximum of 15 cross-links was chosen under the consideration of the number of cross-links the fibers generally have. We found that only a fraction of fibers have a higher number of intersections with other fibers. However, we investigated the effect of a 10% or 20% change in this parameter and found that it has little impact (see Fig. S8).

Computational simulation algorithm

Using a time step of 3 s in the simulation process, the procedure between each time step can be summarized as follows:

Step 1: For each fiber, we determine whether a cell has exerted a force on it during the last time step. The fibers are reorientated as explained in Eq. 2.

Step 2: We find all of the fibers that are in contact with a cell and establish whether the cell has front-rear polarity. If this is the case, we calculate the polarity axis using Eq. S5 of the Supporting Material.

Step 3: If the cell has front-rear polarity, we calculate the net force from Eq. S6 that will lead to its movement on the matrix.

Step 4: We move each cell according to the forces calculated in step 3 by solving Eq. 1, which is numerically solved by using the forward Euler method.

This procedure is illustrated schematically in Fig. S1.

Data analysis

To compare our results with experimental data, we use the cell speed and persistence time as measures, as is done in many experimental setups (37–40). The persistence time can be calculated by providing a fit of the experimentally obtained mean-squared displacements to the mean-squared displacements given by the persistent random walk model

$$\langle \delta(t)^2 \rangle = 2s^2P\left[t - P\left(1 - e^{-t/P}\right)\right], \quad (3)$$

where s is the cell speed, P is the persistence time, and $\delta(t)^2$ is the mean-squared displacement. A derivation of this

formula can be found elsewhere (41–43). The mean-squared displacements are calculated from the cell track data of the simulations using the method of nonoverlapping intervals as described by Dickinson and Tranquillo (41) and Harms et al. (37). Given N consecutive positions of the cell with constant time interval Δt, according to this method, the mean-squared displacement $\delta(t_i)^2$ during a time interval of length $t_i = i\Delta t$ is calculated by

$$\left\langle \delta(t_i)^2 \right\rangle = \frac{1}{n_i} \sum_{j=1}^{n_i} \left[\delta_{(1+i(j-1))\Delta t \to (1+ij)\Delta t} \right]^2, \qquad (4)$$

where $i = [1, 2, \ldots, N-1]$ and $n_1 = (N-1)/i$.

In our model, we study cell migration in an in vitro situation where no external chemical gradients and no growth factors exist. However, in most published migration experiments, the cells were kept in serum, which most likely influenced the migratory behavior of the cells. Therefore, we chose to use a specific set of experiments conducted by Harms et al. (37) to compare the simulation results with results obtained when the cells were serum-starved and resuspended in serum-free medium before migration assays were done. During the migration assays, the cells were tracked for 6 hr and imaged every 15 min. To obtain comparable data, we also used a time interval Δt of 15 min.

The maximum cell speed is a parameter in the model, but as in the previous data analysis (37), the actual cell speed is calculated as an average speed by dividing the root mean-squared displacement in the time interval for $i = 1$ by $\Delta t = 15$ min. This speed is then substituted into the persistent random walk model to fit the persistence time for each cell's data using an unconstrained nonlinear optimization routine (see Supporting Material for full details).

RESULTS

In these single-cell migration simulations, we initially ignored the added noise term. At the beginning of all simulations, we placed a nonpolarized cell in the middle of a 1000×1000 μm area of ECM. The cell was then left to polarize and start migrating over a time of 3 hr, and was then tracked over 6 hr of real time to make it comparable to experiments that were run for the same length of time (37). All parameter values used in the simulations are given in Table S1.

Influence of matrix stiffness on persistence and migration speed

First we investigated the effect of matrix stiffness on cell migration. We ran 15 simulations for each of the following cases in which we varied the matrix composition: 1), a very loose matrix ($S = 0$); 2), a medium-stiff matrix ($S = 0.5$); and 3), a very stiff matrix that cannot be reorientated ($S = 1$). In addition, we ran 15 simulations in which the stiffness was calculated individually for each fiber as explained above. We did this for four different matrix architectures by seeding the random number generator, which is used to place the matrix fibers, with four different numbers. The random number generator used for the noise terms in the cell movement was given the same 15 seeds in the four studies. The results are given in Fig. 3, with outliers denoted by small circles.

It can be seen from Fig. 3 that the persistence times on a stiff matrix have the largest variation over the four different sets of simulations, which means that the tracks of cells on a stiff matrix are the most dependent on the matrix architecture. This is not unexpected. The least variation can be seen over the simulations in which the stiffness of the matrix is calculated for each fiber independently. Here we get persistence times between 3 and 109 min (apart from one outlier, which has a persistence time of 245 min), with the majority (the lower and upper quartiles) being between 20 and 60 min. In their experiments, Harms et al. (37) measured a persistence time of roughly 8–20 min in Chinese hamster ovary cells on fibronectin unstimulated by epidermal growth factor (EGF), and a persistence time of ~19 to 50 min in cells stimulated by EGF (cf. Fig. 2 *D* in Harms et al. (37)). Thus, although our simulations predict a slightly higher persistence time than is observed in unstimulated cells, we do get values of the right order of magnitude. It is clear from the results, however, that the reorientation of the matrix fibers is crucial for this. Similar values as mentioned above were also found for a matrix stiffness of 0.5 and a very loose matrix, but a stiff matrix that allows no reorientation gives much more variation and much higher persistence times than observed in the experiments. A more detailed study of the persistence time and mean actual speed of migration of an individual cell on matrices of varying stiffness S between 0.5 and 1 can be found in the Supporting Material. Interestingly, in all simulations we found that cells on a very stiff matrix move significantly more slowly than cells on a matrix that allows reorientation (Fig. 3, *e–h,* and Fig. S4 *b*). Presumably, this is because the cells are in contact with fewer matrix fibers in this case. This follows from the fact that in soft matrices, the reorientation allows for the contacts between the fiber and the cell to be preserved for a longer time. Whether this will also be true in experiments remains to be seen, although the results of Lo et al. (18) appear to substantiate this.

We can also track the cells over longer time periods and see that they exhibit a random walk behavior. We did this over 3 days. For these simulations, we used the random number generator seed for the stochasticity in the cell movement that gave us the median persistence time for cells on a very stiff matrix and also on a matrix where we calculated the stiffness for each fiber independently (Fig. 4). Here again, the difference becomes clear between the path of a cell that reorients the matrix (Fig. 4 *b*) and that of a cell

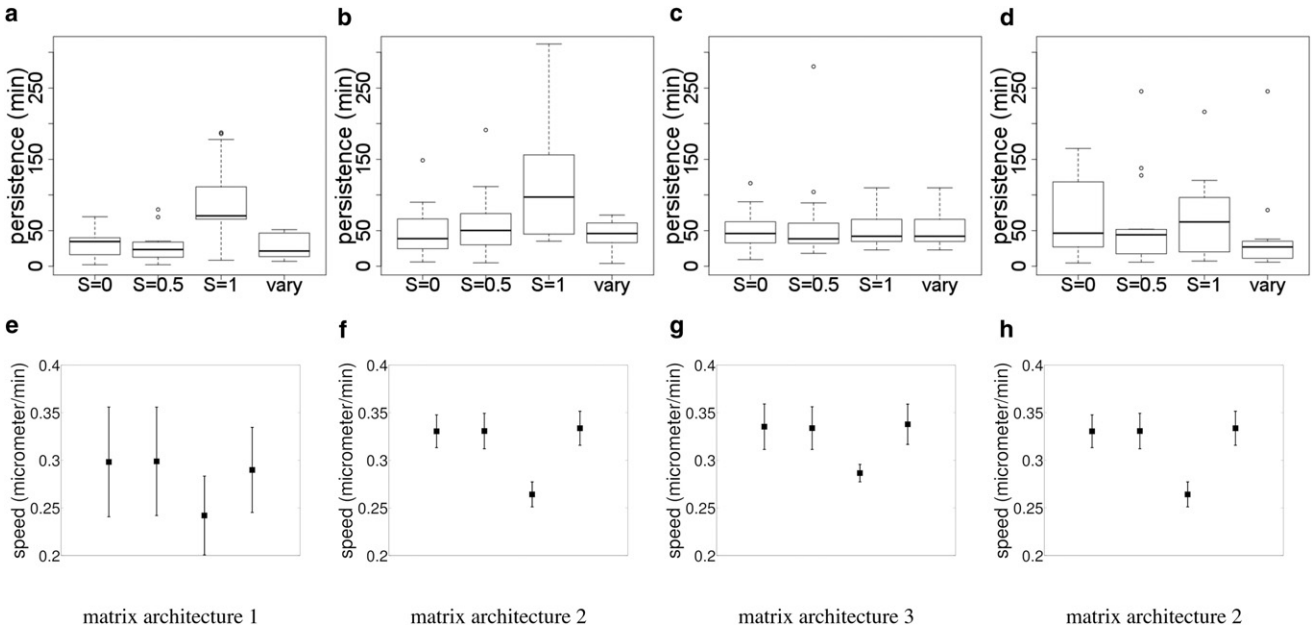

FIGURE 3 Plots showing how the persistence time and mean actual speed of cell migration vary with different matrix stiffnesses in the four different matrix architectures. Each matrix architecture is produced by using a different seed for the random number generator that gives rise to the position and orientation of the matrix fibers. (*a–d*) Plots showing the persistence time in minutes for cells on loose ($S = 0$), medium-stiff ($S = 0.5$), and stiff ($S = 1$) matrices, as well as for stiffness depending on matrix interconnectedness at a given point. In plot *d* two outliers exist outside of the *y* axis range for $S = 0$, at 367.24 min and 430.87 min, respectively. The four boxplots represent the results of cell migration on four different matrix architectures for 15 simulations for each stiffness per architecture. (*e–h*) Plots showing the actual mean speed of the cells during the simulations that led to the boxplots above.

that does not (Fig. 4 *a*). When matrix reorientation occurs, it leads to very sharp, nonsmooth turns in the cell path (denoted with *green asterisks* in the image). For videos of these simulations, see Movie S1 and Movie S2.

Is cell movement guided by substrate rigidity?

Experiments carried out by Lo et al. (18) showed that individual cell movement can be guided solely by physical interactions between the cells and the underlying substrate. 3T3 fibroblasts were placed in the middle of a collagen-coated polyacrylamide substrate sheet, half of which was soft and the other half of which was stiff. The results showed that the cells either migrated onto the stiffer side when they started on the soft side or stayed on the stiff side when they started there (see Fig. 5), i.e., cells tend to prefer stiff matrices to softer ones. This apparent preference for a stiff substrate is termed durotaxis.

These experimental results provide us with a scenario to test with our modeling approach. We created a 2D domain similar to that used by Lo et al. (18) with a different stiffness of matrix in each half, creating a transition of rigidity across the middle. This configuration is shown in Fig. 6 *a*. A single cell is placed close to the transition zone (indicated by a *red asterisk* in Fig. 6, *b–e*). Initially we assigned the left side of the matrix a stiffness of 0.25 and the right side of the matrix a stiffness of 0.75, which meant that the cell started out on the stiffer side. We then ran 15 simulations over 3 days of real time using this configuration and noted the final location of the cell in the domain. We then switched the stiffness properties around, leading to the cell starting on the softer side, as the right side of the matrix was now assigned a stiffness value of 0.25 and the left side a value of 0.75. The results are shown in Fig. 6, *b* and *c*. It can be seen that there is a slight preference for the stiffer side of the matrix, as the cell stays on the stiffer

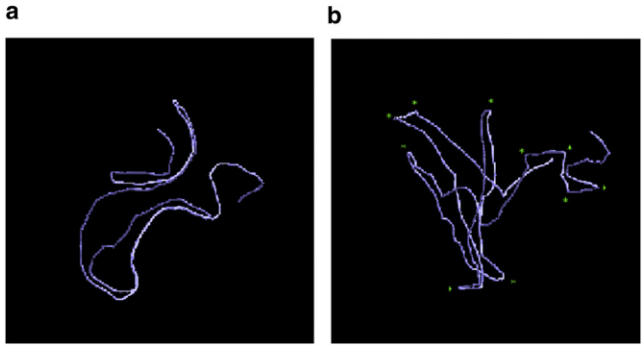

FIGURE 4 Plots showing the cell paths that developed over 3 days (*a*) without and (*b*) with matrix reorientation (using matrix architecture 1 from Fig. 3). In case *b*, the matrix stiffness *S* is dependent on fiber connectedness. The plots show that without matrix reorientation, the cell path is much smoother and does not contain any sharp turns by the cell (*a*). In contrast, with matrix reorientation (*b*), the cell undertakes many more sharp turns and changes of direction, denoted by asterisks. Each black square is an area of 500×500 μm.

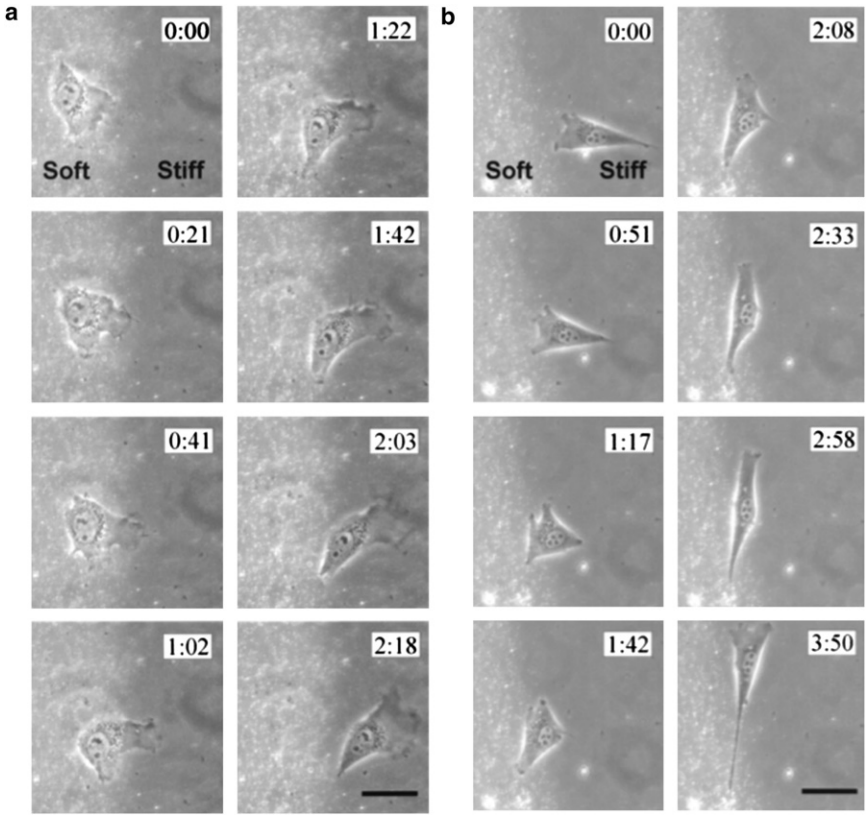

FIGURE 5 Figure showing experiments by Lo et al. (18) in which cells are placed close to the gradient on a matrix with two different stiffnesses. Panel *a* shows a cell that is placed on the softer side of the matrix and then over time migrates onto the stiffer side of the matrix. Panel *b* shows a cell that is placed on the stiffer side of the matrix initially and over time moves toward the gradient but then stays on the stiffer side of the matrix. Reproduced with copyright permission from Lo et al. (18).

side in eight of the 15 simulations where it started on the stiffer side and it moves to the stiffer side in nine of the 15 simulations where it started on the softer side. However, when the discontinuity in rigidity is increased, the results become much clearer, as can be seen in Fig. 6, *d* and *e*. Here the soft side is given a stiffness of 0.05 and the stiff side is given a value of 0.95. In the simulations where the cell starts on this very stiff side, the cell stays on that side in 12 out of the 15 simulations. In the set of simulations where it starts on the soft side, it still ends up on the stiffer side in 13 out of the 15 simulations. Qualitatively, these results mirror those found by Lo et al. (18), i.e., there is an apparent preference of cells for a stiff substrate. Our simulation results indicate that the reorientation of the matrix (or the lack thereof) on stiffer matrices may play an important role in durotaxis.

The fact that we are able to reproduce these results by using our computational model suggests that the physical structure of the ECM is a sufficient condition for a cell to choose a particular location within the surrounding environment. It is difficult to conclude this from biological observations alone, because in experiments the internal cell dynamics, internal cell biomechanics, cell phenotypic properties, etc., are all factors that could possibly play a role, and these cannot be ignored experimentally. In our model, the location of the cell depends uniquely on the physical structure of the matrix and on the cell movement, and our findings suggest that these are sufficient to explain the cells' preference for stiffer matrices.

Nonlinear dependencies of persistence time and cell speed on matrix composition and architecture

To investigate the influence of cell speed and matrix characteristics on the persistence time, we ran a number of simulations of cells migrating on matrices, where the cells were given different maximum cell speeds (denoted by s_{max}) and the composition of the matrices was varied in terms of different fiber lengths and densities. In all of these simulations we calculated the matrix stiffness independently for each fiber as explained above, and used the first matrix architecture from the previous simulations. In the first set we increased s_{max} from 10 μm/hr to 20 μm/hr in steps of 2.5 μm/hr. At the same time we varied the matrix fiber length between 25 μm and 100 μm in steps of 12.5 μm, whereby the number of matrix fibers was always increased or decreased accordingly so that the overall density of matrix fibers was not altered. For each combination, 10 simulations were run and the persistence times and mean actual speed were calculated. The results are shown in Fig. 7. The plots in Fig. 7 *a* show that in the case of slow cells (maximum speeds of 10, 12.5, and 15 μm/hr), the cells that migrate on shorter fibers are more persistent than those

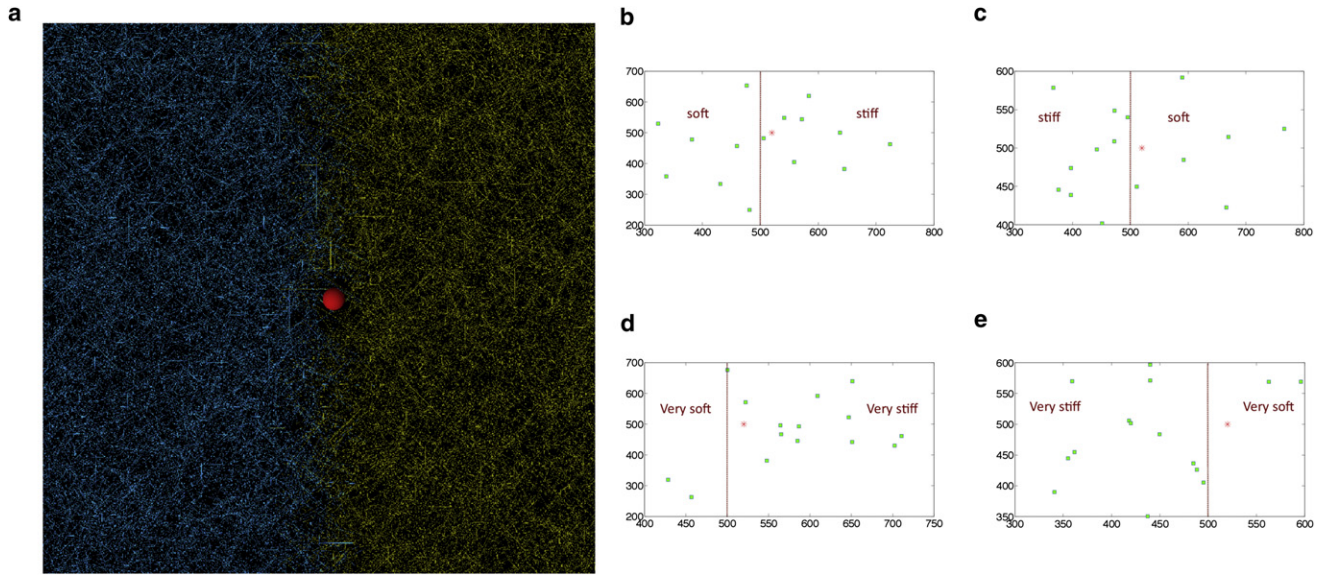

FIGURE 6 (*a*) Matrix is divided into two sides of different stiffnesses on the left and right sides of the domain, with the cell being placed initially just on the right side of the domain (different stiffnesses are denoted by different colors in the online version). The cell is always placed initially in the same position, but the matrix properties are altered. We ran simulations with the left side of the matrix being soft and very soft, and the right side being stiff and very stiff, and vice versa. (*b–e*) Simulation results. The squares are endpoints of the cells after 3 days, and the asterisks show the cells' starting position. Panels *b* and *c* show a slight preference for the stiffer matrix, whereas panels *d* and *e* show that with an increase in the discontinuity in rigidity, this preference increases dramatically, with the cells ending on the stiffer substrate after most simulations independently of their starting position.

that migrate on longer fibers. For maximum cell speeds of 17.5 and 20 μm/hr, fiber length becomes less important and persistence times are more or less independent of fiber length. However, from the plot in Fig. 7 *b*, it appears that the mean actual speed of the cells depends in a bimodal manner on the fiber length.

In the second set of simulations we again increased the cell speed from 10 μm/hr to 20 μm/hr in steps of 2.5 μm/hr. However, this time we changed the matrix density by varying the total number of fibers in the domain. Specifically, we placed a number of fibers of length 75 μm, ranging from a total of 7500 to 22,500 increased by steps of 3750, in the domain of size 1000×1000 μm. We again ran 10 simulations for each combination and calculated the persistence times and the mean actual speed. The results can be seen in Fig. 8. The plots in Fig. 8 *a* show that for cells moving at low maximum speeds (10, 12.5, and 15 μm/hr), there is an increase in persistence with the density before there is a drop at the highest density (22,500 fibers in the domain). For high maximum cell speeds (17.5 and 20 μm/hr), this effect is lost and the persistence times are more or less independent of matrix density. In the plot

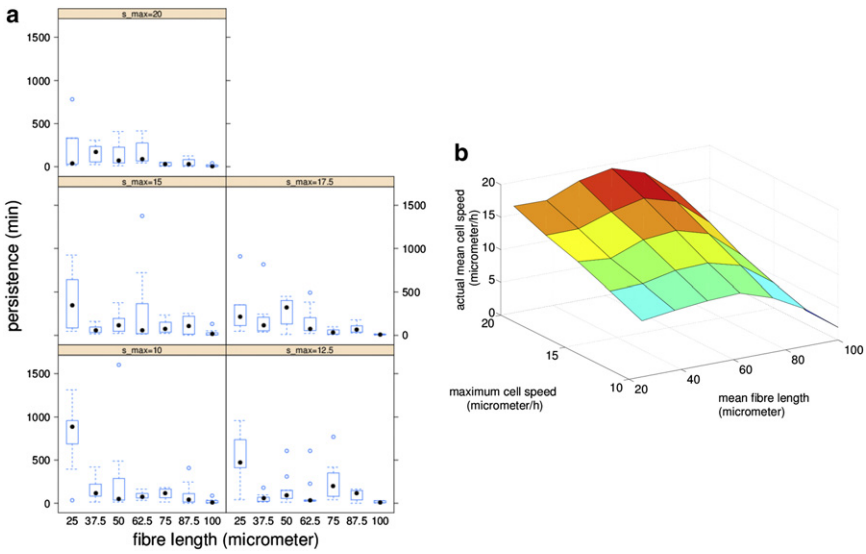

FIGURE 7 Plots showing how the persistence time and actual mean speed of cell migration vary with matrix fiber length and maximum cell speed. (*a*) Boxplot of the persistence time in minutes varying with maximum cell speed and mean fiber length. (*b*) Plot of the mean actual cell speed during the same simulations varying with maximum cell speed and mean fiber length.

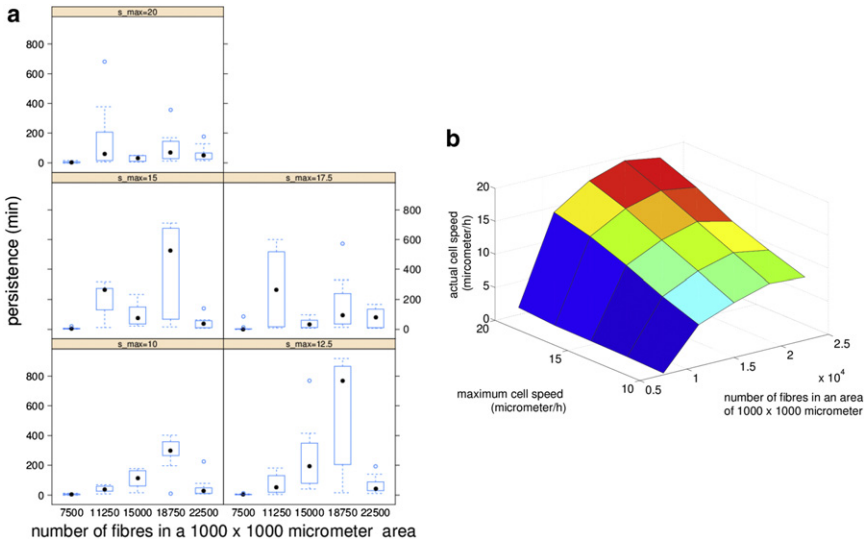

FIGURE 8 Plots showing how the persistence time and mean actual speed of cell migration vary with matrix density and maximum cell speed. (*a*) Boxplot of the mean persistence time in minutes varying with maximum cell speed and matrix density (i.e., the number of matrix fibers). (*b*) Plot of the mean actual cell speed during the same simulations varying with maximum cell speed and matrix density.

shown in Fig. 8 *b*, the actual cell speed clearly shows a biphasic dependence on the matrix density, as previously observed in experiments (44).

Finally, we investigated the behavior of cells on matrices of varying degrees of anisotropy. Specifically, we compared the persistence of cells on a random matrix with that obtained on a biased matrix and a fully aligned matrix (see Fig. 2 for the initial conditions of each type of matrix). We ran 15 simulations for each matrix type and examined the cell tracks in each case. Representative plots are given in Fig. 9. When one compares the cell tracks in each plot, one can see that on average the cells persist in a given direction for a longer period of time on the aligned and biased matrices than on the random (isotropic) matrices. These results indicate that persistence in a given direction (unsurprisingly) decreases with matrix randomness. A formal analysis using the persistence time calculated from Eq. 3 was not possible, because this equation can only be used for motion on isotropic environments.

Sensitivity to the noise terms

The noise term in the calculation of the cell's polarity axis, as well as the noise term $\mathbf{f}_j(t)$, could potentially have a big influence on the persistence of the cell movement. Therefore, we investigated these terms in more detail by running multiple sets of simulations with varying SDs, and the results showed that the influence was negligible. More details on this can be found in the Supporting Material.

Modeling two cells migrating: following the leader

It is frequently observed in experiments that cells follow each other when migrating across a matrix. In three dimensions, this multicellular streaming (45) is well described, and it is clear that it is a very efficient way for cells to migrate along the tracks and tubes of individual leader cells. However, to our knowledge, it also occurs in 2D migration, and it appears naturally during simulations of our model. In Fig. 10 *a*, we kept one cell stationary for a certain time while the neighboring cell was allowed to polarize and start migrating. As soon as the second cell could polarize, it started to follow its former neighbor along the tracks the neighboring cell had laid down (Fig. 10, *b–i*, and Movie S3).

The cell continued to do this until the two cells came into contact, which made the following cell lose its polarized state and repolarize in another direction due to contact inhibition of locomotion, which is encoded in the model. A more detailed analysis of the length of time that cells spend following each other is given in the Supporting Material,

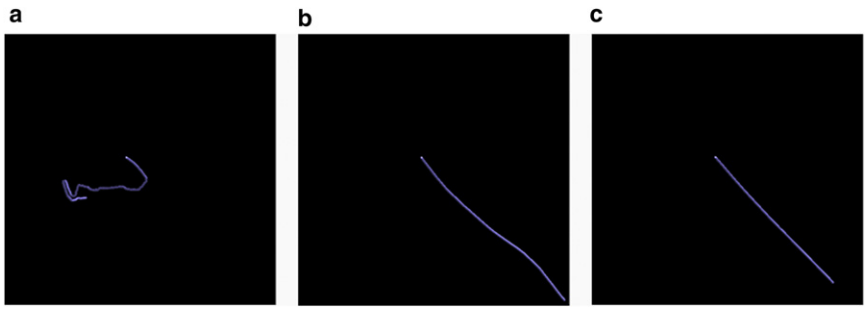

FIGURE 9 Plots of cell tracks over a period of 6 hr on extracellular matrices with (*a*) randomly distributed fibers, (*b*) biased fibers, and (*c*) aligned fibers.

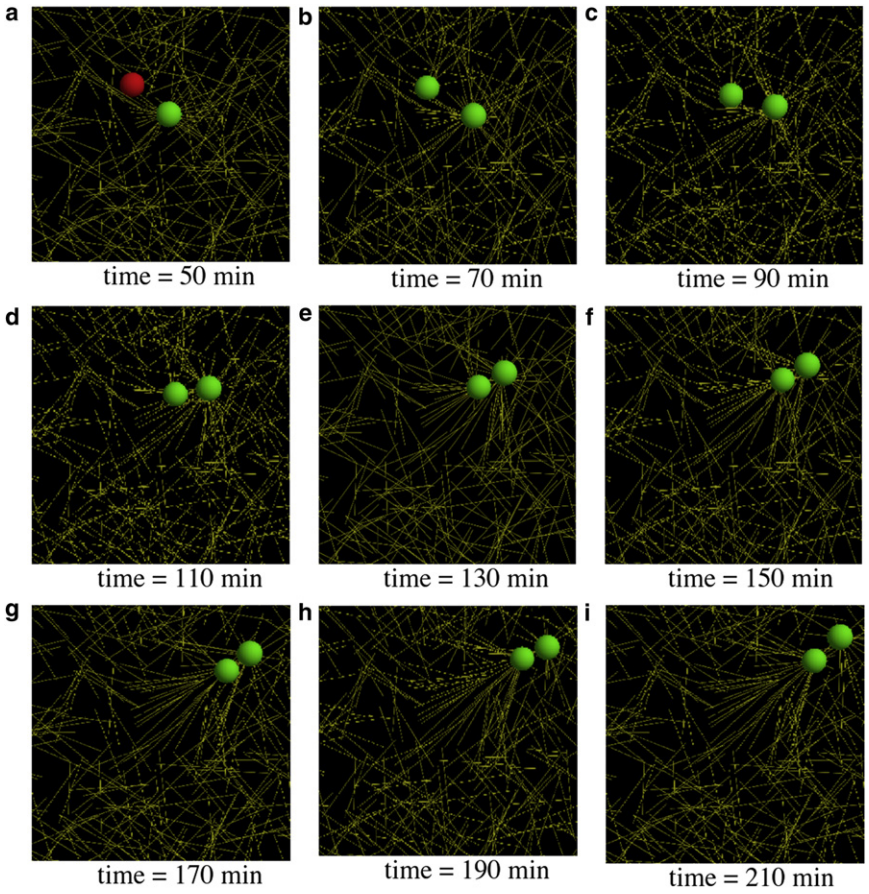

FIGURE 10 Plots showing snapshots at times $t = 50$–210 min of two cells following each other through the matrix. Lighter gray denotes a front-rear polarized cell (green in the online version), and dark gray denotes a nonpolarized cell (red in the online version). The plots show that an initially nonpolarized cell ($t = 50$ min) becomes polarized ($t = 70$ min) and then follows the path of the initially polarized cell.

where we calculate the time that cells spend closer than two cell radii together under different conditions. The results in, Fig. S9 show that stiffer matrices allow for longer episodes of this behavior than do softer ones.

DISCUSSION

We have presented a modeling framework for cell migration on 2D matrices in which both the cell and the matrix fibers are individual elements or agents. Using this approach, we were able to investigate the influence of matrix stiffness on cell migration. We found that the reorientation of the matrix fibers due to cell traction forces may be an important part of this process, because very stiff, nonreorientable matrices led to very variable and occasionally very high persistence times, which does not agree with experiments. We also ran simulations to test whether our model could reproduce experiments that showed a preference of cells for stiffer matrices. The results agreed with those experiments and suggest that matrix reorientation (or the lack thereof) on stiff matrices may be an important factor in durotaxis. Furthermore, we examined the relationships between 1), the persistence time and the maximum cell speed and matrix fiber length or matrix density; and 2), the actual cell speed and the maximum cell speed and matrix fiber length or matrix density. In both cases, we found that there is a nonlinear dependency of the persistence on the two factors, especially at low cell speeds, as well as a biphasic dependency of the actual cell speed on the fiber length and matrix density. Additionally, we looked at the influence of the matrix structure on the persistence time and found that, unsurprisingly, a more ordered matrix leads to higher persistence. We also investigated the stability of the results depending on both noise terms that influence the movement of the cell, and found that they do not have a significant influence on the persistence times measured. Finally, we studied the migration of two cells and found that, as in experiments, cells tend to follow each other under certain conditions. One factor that influences this behavior positively seems to be matrix stiffness.

In this model, the focus is on the most fundamental processes underlying cell migration at the level of cell-matrix interactions. Naturally, certain simplifications are therefore made. For example, we model the ECM as rigid cylinders that are not connected. This means that the cell's application of force onto one fiber does not affect other fibers in the closer environment. Similarly, there is no counter force pulling the fibers back into their original place after the cell has moved across them. These are clearly two aspects that might have an impact on the results and

probably also explain why the results we obtained for very loose, medium-stiff, and variably stiff matrices are very similar. The inclusion of matrix elasticity would most likely lead to less realignment in stiffer matrices and thus could alter the results. Nevertheless, we can learn some things from this model and develop some interesting hypotheses, such as that matrix remodeling may play an important part even in 2D migration. Our results also show the nonlinear dependency of persistence time on cell speed and fiber length or matrix density. Because our results are quantitative and measurable in the laboratory, it would be very interesting to see whether our predictions can be confirmed by experiments. This is especially the case because persistence time is often used to characterize and compare cellular behaviors, and therefore it is important to understand all of the factors that can influence it in an experimental setting. However, we had to estimate a lot of the parameters used in the model because we could find no such measurements in the experimental literature, especially concerning the forces involved in cell-matrix interactions. Therefore, although the results are a first step toward gaining more insight into this process, the model presented here should be seen mainly as a framework that can lead to quantitative results given real experimental input data.

Many studies in the last few years have focused on modeling and understanding cell migration in 3D matrices because such matrices are closer to an in vivo situation, and it has been shown that migration in two dimensions differs significantly from migration in 3D substrates (46). We believe, however, that it is important to study the influence of individual fibers on cell migration in a 2D system first, because effects such as proteolysis can be neglected in this setting. Experimental results have already shown that substrate rigidity (18), fiber alignment (14,19), and cell adhesion and force generation (16) are all important factors in controlling the migration of individual cells on 2D surfaces. Indeed, it is now clear that the biomechanical properties of cells and their environment have as much influence on cell fate and function as do soluble molecular factors. Nonetheless, much remains to be learned about cell migration on 2D surfaces, and we believe that the individual force-based modeling approach adopted here can lead to some ideas about as-yet-unknown factors involved in this process that might be of interest.

It would be very interesting to develop this approach further to model cell migration in 3D matrices and investigate whether modeling individual fibers in this setting can add to our understanding of this process. The addition of explicit external cues and matrix elasticity to the model will help get us one step closer to an in vivo situation. The model can further be extended to a multiscale model by including signaling dynamics of integrins and other receptor molecules. Such a model can then be used to model single-cell as well as multicell migration in various biological contexts. As mentioned in the Introduction, wound healing is partly driven by cell migration, and with this type of model we could try to get a better understanding of this process and what is missing or not functioning properly in chronic wounds and other wound-healing disorders. In future work, this model could also be applied to cancer cell invasion and the formation of metastasis. Through this quantitative modeling approach, we hope to be able to predict the spread of cancer cells depending on their environment and mutations.

Thus, in addition to providing interesting insights into cell migration itself, this model has great potential for forming the basis of models of varying complexity for different biological applications.

SUPPORTING MATERIAL

More detail on the model description, the parameter values, the influence of certain parameters on the simulation results and the behavior of two cells following each other across the matrix, and reference (47) are available at http://www.biophysj.org/biophysj/supplemental/S0006-3495(12)00869-7.

I.R.-C. received grant MTM2009-13832 (Ministerio de Ciencia y Technologia, Spain). D.K.S. and M.A.J.C. were supported by European Research Council Advanced Investigator Grant 227619, M5CGS (From Mutations to Metastases: Multiscale Mathematical Modelling of Cancer Growth and Spread) and a Scottish Universities Life Sciences Alliance PhD Studentship.

REFERENCES

1. Lauffenburger, D. A., and A. F. Horwitz. 1996. Cell migration: a physically integrated molecular process. *Cell.* 84:359–369.
2. Yang, J., and R. A. Weinberg. 2008. Epithelial-mesenchymal transition: at the crossroads of development and tumor metastasis. *Dev. Cell.* 14:818–829.
3. Baum, B., J. Settleman, and M. P. Quinlan. 2008. Transitions between epithelial and mesenchymal states in development and disease. *Semin. Cell Dev. Biol.* 19:294–308.
4. Lee, J. M., S. Dedhar, …, E. W. Thompson. 2006. The epithelial-mesenchymal transition: new insights in signaling, development, and disease. *J. Cell Biol.* 172:973–981.
5. Etienne-Manneville, S. 2008. Polarity proteins in migration and invasion. *Oncogene.* 27:6970–6980.
6. Tanos, B., and E. Rodriguez-Boulan. 2008. The epithelial polarity program: machineries involved and their hijacking by cancer. *Oncogene.* 27:6939–6957.
7. Huttenlocher, A. 2005. Cell polarization mechanisms during directed cell migration. *Nat. Cell Biol.* 7:336–337.
8. Mogilner, A. 2009. Mathematics of cell motility: have we got its number? *J. Math. Biol.* 58:105–134.
9. Zamir, E., and B. Geiger. 2001. Molecular complexity and dynamics of cell-matrix adhesions. *J. Cell Sci.* 114:3583–3590.
10. Friedl, P., and K. Wolf. 2003. Tumour-cell invasion and migration: diversity and escape mechanisms. *Nat. Rev. Cancer.* 3:362–374.
11. Ridley, A. J., M. A. Schwartz, …, A. R. Horwitz. 2003. Cell migration: integrating signals from front to back. *Science.* 302:1704–1709.
12. Friedl, P., and K. Wolf. 2009. Proteolytic interstitial cell migration: a five-step process. *Cancer Metastasis Rev.* 28:129–135.
13. DiMilla, P. A., K. Barbee, and D. A. Lauffenburger. 1991. Mathematical model for the effects of adhesion and mechanics on cell migration speed. *Biophys. J.* 60:15–37.

14. Friedrichs, J., A. Taubenberger, …, D. J. Muller. 2007. Cellular remodelling of individual collagen fibrils visualized by time-lapse AFM. *J. Mol. Biol.* 372:594–607.

15. Ludwig, T., R. Kirmse, …, U. Schwarz. 2008. Probing cellular microenvironments and tissue remodeling by atomic force microscopy. *Pflugers Arch.* 456:29–49.

16. Kirmse, R., H. Otto, and T. Ludwig. 2011. Interdependency of cell adhesion, force generation and extracellular proteolysis in matrix remodeling. *J. Cell Sci.* 124:1857–1866.

17. Jiang, F., K. Khairy, …, D. J. Müller. 2004. Creating nanoscopic collagen matrices using atomic force microscopy. *Microsc. Res. Tech.* 64:435–440.

18. Lo, C.-M., H.-B. Wang, …, Y. L. Wang. 2000. Cell movement is guided by the rigidity of the substrate. *Biophys. J.* 79:144–152.

19. Poole, K., K. Khairy, …, D. Mueller. 2005. Molecular-scale topographic cues induce the orientation and directional movement of fibroblasts on two-dimensional collagen surfaces. *J. Mol. Biol.* 349: 380–386.

20. Novak, I. L., B. M. Slepchenko, and A. Mogilner. 2008. Quantitative analysis of G-actin transport in motile cells. *Biophys. J.* 95:1627–1638.

21. Mogilner, A., and L. Edelstein-Keshet. 2002. Regulation of actin dynamics in rapidly moving cells: a quantitative analysis. *Biophys. J.* 83:1237–1258.

22. Zaman, M. H., R. D. Kamm, …, D. A. Lauffenburger. 2005. Computational model for cell migration in three-dimensional matrices. *Biophys. J.* 89:1389–1397.

23. Dallon, J. C., J. A. Sherratt, and P. K. Maini. 1999. Mathematical modelling of extracellular matrix dynamics using discrete cells: fiber orientation and tissue regeneration. *J. Theor. Biol.* 199:449–471.

24. McDougall, S., J. Dallon, …, P. Maini. 2006. Fibroblast migration and collagen deposition during dermal wound healing: mathematical modelling and clinical implications. *Philos. Transact. A Math. Phys. Eng. Sci.* 364:1385–1405.

25. Hillen, T. 2006. M^5 mesoscopic and macroscopic models for mesenchymal motion. *J. Math. Biol.* 53:585–616.

26. Chauviere, A., T. Hillen, and L. Preziosi. 2007. Modelling cell movement in anisotropic and heterogeneous networks tissues. *Netw. Heterogen. Media.* 2:333–357.

27. Painter, K. J. 2009. Modelling cell migration strategies in the extracellular matrix. *J. Math. Biol.* 58:511–543.

28. Galle, J., M. Loeffler, and D. Drasdo. 2005. Modeling the effect of deregulated proliferation and apoptosis on the growth dynamics of epithelial cell populations in vitro. *Biophys. J.* 88:62–75.

29. Ramis-Conde, I., D. Drasdo, …, M. A. Chaplain. 2008. Modeling the influence of the E-cadherin-β-catenin pathway in cancer cell invasion: a multiscale approach. *Biophys. J.* 95:155–165.

30. Ramis-Conde, I., M. A. J. Chaplain, …, D. Drasdo. 2009. Multi-scale modelling of cancer cell intravasation: the role of cadherins in metastasis. *Phys. Biol.* 6:016008.

31. Schneider, S. W., P. Pagel, …, A. Schwab. 2000. Volume dynamics in migration epithelial cells measured with atomic force microscopy. *Pflugers Arch.* 439:297–303.

32. Friedl, P., K. Maaser, …, K. S. Zänker. 1997. Migration of highly aggressive MV3 melanoma cells in 3-dimensional collagen lattices results in local matrix reorganization and shedding of α2 and β1 integrins and CD44. *Cancer Res.* 57:2061–2070.

33. Leith, D. 1987. Drag on nonspherical objects. *Aerosol Sci. Technol.* 6:153–161.

34. Payne, L. E., and W. H. Pell. 1959. The Stokes flow problem for a class of axially symmetric bodies. *Fluid Mechanics.* 7:529–549.

35. Lemmon, C. A., C. S. Chen, and L. H. Romer. 2009. Cell traction forces direct fibronectin matrix assembly. *Biophys. J.* 96:729–738.

36. du Roure, O., A. Saez, …, B. Ladoux. 2005. Force mapping in epithelial cell migration. *Proc. Natl. Acad. Sci. USA.* 102:2390–2395 (Erratum in *Proc. Natl. Acad. Sci. U S A.* 2005. 102:14122).

37. Harms, B. D., G. M. Bassi, …, D. A. Lauffenburger. 2005. Directional persistence of EGF-induced cell migration is associated with stabilization of lamellipodial protrusions. *Biophys. J.* 88:1479–1488.

38. Gail, M. H., and C. W. Boone. 1970. The locomotion of mouse fibroblasts in tissue culture. *Biophys. J.* 10:980–993.

39. Bergman, A. J., and K. Zygourakis. 1999. Migration of lymphocytes on fibronectin-coated surfaces: temporal evolution of migratory parameters. *Biomaterials.* 20:2235–2244.

40. Stokes, C. L., D. A. Lauffenburger, and S. K. Williams. 1991. Migration of individual microvessel endothelial cells: stochastic model and parameter measurement. *J. Cell Sci.* 99:419–430.

41. Othmer, H. G., S. R. Dunbar, and W. Alt. 1988. Models of dispersal in biological systems. *J. Math. Biol.* 26:263–298.

42. Alt, W. 1990. Correlation analysis of two-dimensional locomotion paths. *In* Biological Motion. W. Alt and G. Hoffmann, editors. Springer-Verlag, Berlin. 254–268.

43. Dickinson, R. B., and T. Tranquillo. 1993. Optimal estimation of cell movement indices from the statistical analysis of cell tracking data. *AIChE J.* 39:1995–2010.

44. Palecek, S. P., J. C. Loftus, …, A. F. Horwitz. 1997. Integrin-ligand binding properties govern cell migration speed through cell-substratum adhesiveness. *Nature.* 385:537–540.

45. Friedl, P., and K. Wolf. 2010. Plasticity of cell migration: a multiscale tuning model. *J. Cell Biol.* 188:11–19.

46. Doyle, A. D., F. W. Wang, …, K. M. Yamada. 2009. One-dimensional topography underlies three-dimensional fibrillar cell migration. *J. Cell Biol.* 184:481–490.

47. Matsumoto, M., and T. Nishimura. 1998. Mersenne Twister: a 623-dimensionally equidistributed uniform pseudo-random number generator. *ACM Trans. Model. Comput. Simul.* 8:3–30.